DESY 94-154
August 1994

ISSN 0418-9833

A Search for Leptoquarks and Squarks at HERA

H1 Collaboration

Abstract:

A search in the H1 experiment at HERA for scalar and vector leptoquarks, leptogluons and squarks coupling to first generation fermions is presented in a data sample corresponding to an integrated luminosity of 425 nb^{-1}. For masses ranging up to ~ 275 GeV, no significant evidence for the direct production of such particles is found in various possible decay channels. At high masses and beyond the centre of mass energy of 296 GeV a contact interaction analysis is used to further constrain the couplings and masses of new vector leptoquarks and to set lower limits on compositeness scales.

T. Ahmed[3], S. Aid[13], V. Andreev[24], B. Andrieu[28], R.-D. Appuhn[11], M. Arpagaus[36], A. Babaev[26], J. Baehr[35], J. Bán[17], P. Baranov[24], E. Barrelet[29], W. Bartel[11], M. Barth[4], U. Bassler[29], H.P. Beck[37], H.-J. Behrend[11], A. Belousov[24], Ch. Berger[1], H. Bergstein[1], G. Bernardi[29], R. Bernet[36], G. Bertrand-Coremans[4], M. Besançon[9], R. Beyer[11], P. Biddulph[22], J.C. Bizot[27], V. Blobel[13], K. Borras[8], F. Botterweck[4], V. Boudry[28], A. Braemer[14], F. Brasse[11], W. Braunschweig[1], V. Brisson[27], D. Bruncko[17], C. Brune[15], R.Buchholz[11], L. Büngener[13], J. Bürger[11], F.W. Büsser[13], A. Buniatian[11,39], S. Burke[18], G. Buschhorn[26], A.J. Campbell[11], T. Carli[26], F. Charles[11], D. Clarke[5], A.B. Clegg[18], M. Colombo[8], J.G. Contreras[8], J.A. Coughlan[5], A. Courau[27], Ch. Coutures[9], G. Cozzika[9], L. Criegee[11], D.G. Cussans[5], J. Cvach[30], S. Dagoret[29], J.B. Dainton[19], M. Danilov[23], W.D. Dau[16], K. Daum[34], M. David[9], E. Deffur[11], B. Delcourt[27], L. Del Buono[29], A. De Roeck[11], E.A. De Wolf[4], P. Di Nezza[32], C. Dollfus[37], J.D. Dowell[3], H.B. Dreis[2], J. Duboc[29], D. Düllmann[13], O. Dünger[13], H. Duhm[12], J. Ebert[34], T.R. Ebert[19], G. Eckerlin[11], V. Efremenko[23], S. Egli[37], H. Ehrlichmann[35], S. Eichenberger[37], R. Eichler[36], F. Eisele[14], E. Eisenhandler[20], R.J. Ellison[22], E. Elsen[11], M. Erdmann[14], W. Erdmann[36], E. Evrard[4], L. Favart[4], A. Fedotov[23], D. Feeken[13], R. Felst[11], J. Feltesse[9], J. Ferencei[15], F. Ferrarotto[32], K. Flamm[11], M. Fleischer[11], M. Flieser[26], G. Flügge[2], A. Fomenko[24], B. Fominykh[23], M. Forbush[7], J. Formánek[31], J.M. Foster[22], G. Franke[11], E. Fretwurst[12], E. Gabathuler[19], K. Gabathuler[33], K. Gamerdinger[26], J. Garvey[3], J. Gayler[11], M. Gebauer[8], A. Gellrich[13], H. Genzel[1], R. Gerhards[11], U. Goerlach[11], L. Goerlich[6], N. Gogitidze[24], M. Goldberg[29], D. Goldner[8], B. Gonzalez-Pineiro[29], A.M. Goodall[19], I. Gorelov[23], P. Goritchev[23], C. Grab[36], H. Grässler[2], R. Grässler[2], T. Greenshaw[19], G. Grindhammer[26], A. Gruber[26], C. Gruber[16], J. Haack[35], D. Haidt[11], L. Hajduk[6], O. Hamon[29], M. Hampel[1], E.M. Hanlon[18], M. Hapke[11], W.J. Haynes[5], J. Heatherington[20], V. Hedberg[21], G. Heinzelmann[13], R.C.W. Henderson[18], H. Henschel[35], R. Herma[1], I. Herynek[30], M.F. Hess[26], W. Hildesheim[12], P. Hill[5], K.H. Hiller[35], C.D. Hilton[22], J. Hladký[30], K.C. Hoeger[22], M. Höppner[8], R. Horisberger[33], Ph. Huet[4], H. Hufnagel[14], M. Ibbotson[22], H. Itterbeck[1], M.-A. Jabiol[9], A. Jacholkowska[27], C. Jacobsson[21], M. Jaffre[27], J. Janoth[15], T. Jansen[11], L. Jönsson[21], K. Johannsen[13], D.P. Johnson[4], L. Johnson[18], H. Jung[11], P.I.P. Kalmus[20], D. Kant[20], R. Kaschowitz[2], P. Kasselmann[12], U. Kathage[16], H.H. Kaufmann[35], S. Kazarian[11], I.R. Kenyon[3], S. Kermiche[27], C. Keuker[1], C. Kiesling[26], M. Klein[35], C. Kleinwort[13], G. Knies[11], W. Ko[7], T. Köhler[1], H. Kolanoski[8], F. Kole[7], S.D. Kolya[22], V. Korbel[11], M. Korn[8], P. Kostka[35], S.K. Kotelnikov[24], M.W. Krasny[6,29], H. Krehbiel[11], D. Krücker[2], U. Krüger[11], U. Krüner-Marquis[11], J.P. Kubenka[26], H. Küster[2], M. Kuhlen[26], T. Kurča[17], J. Kurzhöfer[8], B. Kuznik[34], D. Lacour[29], F. Lamarche[28], R. Lander[7], M.P.J. Landon[20], W. Lange[35], P. Lanius[26], J.-F. Laporte[9], A. Lebedev[24], C. Leverenz[11], S. Levonian[11,24], Ch. Ley[2], A. Lindner[8], G. Lindström[12], F. Linsel[11], J. Lipinski[13], B. List[11], P. Loch[27], H. Lohmander[21], G.C. Lopez[20], D. Lüke[8,11], N. Magnussen[34], E. Malinovski[24], S. Mani[7], R. Maraček[17], P. Marage[4], J. Marks[25], R. Marshall[22], J. Martens[34], R. Martin[19], H.-U. Martyn[1], J. Martyniak[6], S. Masson[2], T. Mavroidis[20], S.J. Maxfield[19], S.J. McMahon[19], A. Mehta[22], K. Meier[15], D. Mercer[22], T. Merz[11], C.A. Meyer[37], H. Meyer[34], J. Meyer[11], S. Mikocki[6], D. Milstead[19], F. Moreau[28], J.V. Morris[5], G. Müller[11], K. Müller[37], P. Murín[17], V. Nagovizin[23], R. Nahnhauer[35], B. Naroska[13], Th. Naumann[35], P.R. Newman[3], D. Newton[18], D. Neyret[29], H.K. Nguyen[29], F. Niebergall[13], C. Niebuhr[11], R. Nisius[1], G. Nowak[6], G.W. Noyes[5], M. Nyberg-Werther[21], H. Oberlack[26], U. Obrock[8], J.E. Olsson[11], E. Panaro[12], A. Panitch[4], C. Pascaud[27], G.D. Patel[19], E. Peppel[11], E. Perez[9], J.P. Phillips[22], Ch. Pichler[12], D. Pitzl[36], G. Pope[7], S. Prell[11], R. Prosi[11], G. Rädel[11], F. Raupach[1], P. Reimer[30], S. Reinshagen[11], P. Ribarics[26], V. Riech[12], J. Riedlberger[36], S. Riess[13], M. Rietz[2], S.M. Robertson[3], P. Robmann[37], H.E. Roloff[35], R. Roosen[4], K. Rosenbauer[1] A. Rostovtsev[23], F. Rouse[7], C. Royon[9], K. Rüter[26], S. Rusakov[24], K. Rybicki[6], R. Rylko[20], N. Sahlmann[2], E. Sanchez[26], D.P.C. Sankey[5], M. Savitsky[23], P. Schacht[26], S. Schiek[11], P. Schleper[14], W. von Schlippe[20], C. Schmidt[11], D. Schmidt[34], G. Schmidt[13], A. Schöning[11], V. Schröder[11], E. Schuhmann[26], B. Schwab[14], A. Schwind[35], U. Seehausen[13], F. Sefkow[11], M. Seidel[12], R. Sell[11], A. Semenov[23], V. Shekelyan[23], I. Sheviakov[24], H. Shooshtari[26], L.N. Shtarkov[24], G. Siegmon[16], U. Siewert[16], Y. Sirois[28], I.O. Skillicorn[10], P. Smirnov[24], J.R. Smith[7], Y. Soloviev[24], H. Spitzer[13], R. Starosta[1], M. Steenbock[13], P. Steffen[11], R. Steinberg[2], B. Stella[32], K. Stephens[22], J. Stier[11], J. Stiewe[15], U. Stösslein[35], J. Strachota[30], U. Straumann[37], W. Struczinski[2], J.P. Sutton[3], S. Tapprogge[15], R.E. Taylor[38,27], V. Tchernyshov[23], C. Thiebaux[28], G. Thompson[20], I. Tichomirov[23], P. Truöl[37], J. Turnau[6], J. Tutas[14], P. Uelkes[2], A. Usik[24], S. Valkár[31], A. Valkárová[31], C. Vallée[25], P. Van Esch[4], P. Van Mechelen[4], A. Vartapetian[11,39], Y. Vazdik[24], M. Vecko[30], P. Verrecchia[9], G. Villet[9], K. Wacker[8], A. Wagener[2], M. Wagener[33], I.W. Walker[18], A. Walther[8], G. Weber[13], M. Weber[11], D. Wegener[8], A. Wegner[11], H.P. Wellisch[26], L.R. West[3], S. Willard[7], M. Winde[35], G.-G. Winter[11], A.E. Wright[22], E. Wünsch[11], N. Wulff[11], T.P. Yiou[29], J. Žáček[31], D. Zarbock[12], Z. Zhang[27], M. Zimmer[11], W. Zimmermann[11], F. Zomer[27], and K. Zuber[15]

[1] *I. Physikalisches Institut der RWTH, Aachen, Germany*[a]
[2] *III. Physikalisches Institut der RWTH, Aachen, Germany*[a]
[3] *School of Physics and Space Research, University of Birmingham, Birmingham, UK*[b]
[4] *Inter-University Institute for High Energies ULB-VUB, Brussels; Universitaire Instellingen Antwerpen, Wilrijk, Belgium*[c]
[5] *Rutherford Appleton Laboratory, Chilton, Didcot, UK*[b]
[6] *Institute for Nuclear Physics, Cracow, Poland*[d]
[7] *Physics Department and IIRPA, University of California, Davis, California, USA*[e]
[8] *Institut für Physik, Universität Dortmund, Dortmund, Germany*[a]
[9] *CEA, DSM/DAPNIA, CE-SACLAY, Gif-sur-Yvette, France*
[10] *Department of Physics and Astronomy, University of Glasgow, Glasgow, UK*[b]
[11] *DESY, Hamburg, Germany*[a]
[12] *I. Institut für Experimentalphysik, Universität Hamburg, Hamburg, Germany*[a]
[13] *II. Institut für Experimentalphysik, Universität Hamburg, Hamburg, Germany*[a]
[14] *Physikalisches Institut, Universität Heidelberg, Heidelberg, Germany*[a]
[15] *Institut für Hochenergiephysik, Universität Heidelberg, Heidelberg, Germany*[a]
[16] *Institut für Reine und Angewandte Kernphysik, Universität Kiel, Kiel, Germany*[a]
[17] *Institute of Experimental Physics, Slovak Academy of Sciences, Košice, Slovak Republic*
[18] *School of Physics and Materials, University of Lancaster, Lancaster, UK*[b]
[19] *Department of Physics, University of Liverpool, Liverpool, UK*[b]
[20] *Queen Mary and Westfield College, London, UK*[b]
[21] *Physics Department, University of Lund, Lund, Sweden*[f]
[22] *Physics Department, University of Manchester, Manchester, UK*[b]
[23] *Institute for Theoretical and Experimental Physics, Moscow, Russia*
[24] *Lebedev Physical Institute, Moscow, Russia*
[25] *CPPM, Université d'Aix-Marseille II, IN2P3-CNRS, Marseille, France*
[26] *Max-Planck-Institut für Physik, München, Germany*[a]

[27] *LAL, Université de Paris-Sud, IN2P3-CNRS, Orsay, France*
[28] *LPNHE, Ecole Polytechnique, IN2P3-CNRS, Palaiseau, France*
[29] *LPNHE, Universités Paris VI and VII, IN2P3-CNRS, Paris, France*
[30] *Institute of Physics, Czech Academy of Sciences, Praha, Czech Republic*[g]
[31] *Nuclear Center, Charles University, Praha, Czech Republic*[g]
[32] *INFN Roma and Dipartimento di Fisica, Universita "La Sapienza", Roma, Italy*
[33] *Paul Scherrer Institut, Villigen, Switzerland*
[34] *Fachbereich Physik, Bergische Universität Gesamthochschule Wuppertal, Wuppertal, Germany*[a]
[35] *DESY, Institut für Hochenergiephysik, Zeuthen, Germany*[a]
[36] *Institut für Teilchenphysik, ETH, Zürich, Switzerland*[h]
[37] *Physik-Institut der Universität Zürich, Zürich, Switzerland*[h]
[38] *Stanford Linear Accelerator Center, Stanford California, USA*
[39] *Visitor from Yerevan Phys.Inst., Armenia*

[a] *Supported by the Bundesministerium für Forschung und Technologie, FRG under contract numbers 6AC17P, 6AC47P, 6DO57I, 6HH17P, 6HH27I, 6HD17I, 6HD27I, 6KI17P, 6MP17I, and 6WT87P*
[b] *Supported by the UK Particle Physics and Astronomy Research Council, and formerly by the UK Science and Engineering Research Council*
[c] *Supported by FNRS-NFWO, IISN-IIKW*
[d] *Supported by the Polish State Committee for Scientific Research, grant No. 204209101*
[e] *Supported in part by USDOE grant DE F603 91ER40674*
[f] *Supported by the Swedish Natural Science Research Council*
[g] *Supported by GA ČR, grant no. 202/93/2423 and by GA AV ČR, grant no. 19095*
[h] *Supported by the Swiss National Science Foundation*

1 Introduction

The ep collider HERA, in which 26.7 GeV electrons collide with 820 GeV protons, provides access to an as yet unexplored mass domain for the discovery of new particles. Especially promising, given the unique initial state, are searches for heavy particles coupling to either electron–quark pairs such as squarks and leptoquarks or to electron–gluon pairs such as leptogluons. These new particles could be produced singly as s-channel resonances by the fusion of the initial state lepton and a coloured partonic constituent of the proton. In the case of squarks, such production involves a lepton number violating Yukawa coupling as present in the R-parity violating ($\not{R}_p$) supersymmetric extension of the Standard Model (SM). For masses beyond the kinematic limit of $\sqrt{s} = 296$ GeV, interference effects from virtual exchange of new particles may still lead to observable deviations from SM predictions.

This paper combines a direct search for leptoquarks, leptogluons and squarks with a search for indirect effects studied in the general framework of a Contact Interaction (CI) parametrization. The squark search includes an analysis of both $\not{R}_p$ decays via Yukawa couplings and gauge decays into a quark and the lightest supersymmetric particle (LSP) which is assumed to be a neutralino. In $\not{R}_p$ models, the LSP is unstable and decays into leptons and quarks. This is at variance from particle searches in the framework of the minimal supersymmetric model (MSSM) where the LSP is necessarily stable leading to events with large missing transverse momentum. The observation of gauge decays would make it possible to distinguish squark from leptoquark production.

The analysis presented here is based on an integrated luminosity of $\mathcal{L} = 425 \pm 21$ nb^{-1} collected during 1993. This represents an increase by a factor ~ 17 compared to the data sample used in earlier searches for leptoquarks and leptogluons at HERA [1, 2].

2 Phenomenology

Leptoquarks are colour triplet bosons carrying lepton and baryon numbers. They appear naturally in various theories beyond the Standard Model, in particular those attempting to provide an explanation for the observed symmetry between the lepton and quark particle multiplets. Examples are Grand Unifying Theories or Superstring motivated E_6 models, but also Compositeness and Technicolour models.

In order to be independent of specific model assumptions, a phenomenological ansatz [3] is used to present the result of our search. The effective Lagrangian considered conserves lepton and baryon number, obeys the symmetries of the SM gauge groups $U(1)_Y$, $SU(2)_L$ and $SU(3)_C$, and includes all possible dimensionless couplings λ of scalar and vector leptoquarks to leptons and quarks. Altogether there are thus 10 different leptoquark isospin multiplets, with couplings to left and right handed fermions (see for example table 2) [1]. A more detailed discussion of the general classification scheme for leptoquarks may be found in our previous publication [1] or in [3, 4].

Given the existing stringent constraints from low energy experiments (for a review see [5]), we restrict our search by the following simplifying assumptions:

- Only couplings to first generation fermions are considered.
- One of the leptoquark multiplets is produced dominantly.
- The states in the leptoquark doublets and triplets are degenerate in mass.
- Non-vanishing couplings exist only to either left- (λ_L) or right-handed (λ_R) leptons (i.e. $\lambda_L \cdot \lambda_R \sim 0$).
- The only possible decay channels lead to fermions, either electron + quark, or neutrino + quark.

Experimentally, leptoquarks would show up predominantly as s-channel resonances (fig. 1a) in the electron–quark scattering sub-process with a cross-section depending to first approximation only on λ^2 and on the quark momentum density in the proton. The decay of the leptoquark into an electron, or a neutrino, and a jet leads to signatures indistinguishable event-by-event from the SM neutral and charged current deep inelastic scattering (DIS). Statistically, the new signal may however be discriminated by the presence of a peak in the invariant mass distribution and by the specific angular distribution of the decay products. This angular decay distribution depends on the spin of the leptoquark. Scalars decay isotropically in their centre of mass system leading to a constant $d\sigma \,/\, dy$ where $y = \frac{1}{2}(1 + cos\theta^*)$ corresponds to the Bjorken scattering variable in DIS and θ^* is

[1] Scalar and vector leptoquarks are denoted by S and V respectively. A superscript L or R means coupling to a left- (L) or right-handed (R) lepton. A subscript gives the weak isospin.

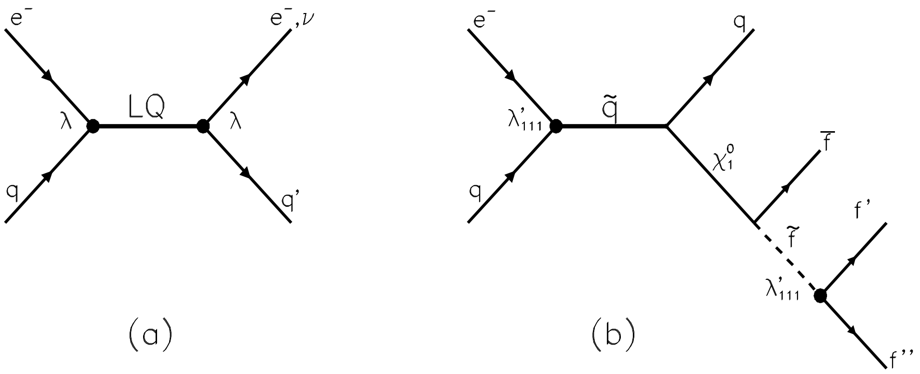

Figure 1: *Lowest order s-channel diagrams for (a) leptoquarks and (b) gauge decays of squarks at HERA. In (b), the $\tilde{f}$ might be a squark or a slepton such that the χ_1^0 decays into a lepton and a $q\bar{q}$ pair.*

the decay polar angle in this reference frame. For vectors $d\sigma\,/\,dy \;\sim\; (1-y)^2$. This is markedly different from the $d\sigma\,/\,dy \sim y^{-2}$ distribution expected for the dominant t-channel photon exchange in neutral current DIS events [2]. The strategy for the leptoquark search is thus to look for DIS–like events at high mass and high y, and to separate them statistically from the standard DIS background.

Leptogluons appear in some composite models [6] as colour octet partners of the known colour singlet leptons where these are bound states of coloured constituents. At HERA they may be produced as s-channel resonances in electron–gluon scattering and may also decay into electron + gluon (like fig. 1a, with quark lines exchanged by gluon lines). Thus their final state signature, an electron and a jet, is very similar to that of leptoquark and neutral current DIS events, but their production cross-sections depend on the compositeness scale Λ [7]. For spin 1/2 leptogluons, the angular decay distribution is $d\sigma\,/\,dy \;\sim\; 1-y$.

Squarks ($\tilde{q}$) are predicted in supersymmetric extensions of the Standard Model as scalar partners of the known quarks, with otherwise identical quantum numbers and couplings to the SM gauge bosons. The general super-potential allows for gauge invariant terms with Yukawa couplings between the new scalar particles and the known fermions [8]. Such couplings are allowed if one assumes the possibility of violating the multiplicatively conserved (e.g. in the MSSM [9]) R-parity, $R_p = (-1)^{3B+L+2S}$ where S denotes the spin, B the baryon number and L the lepton number of the particles.

At HERA specifically the $\not{R}_p$ couplings λ'_{ijk} (where ijk are generation indices) between a lepton, a quark and a squark are of interest [10]. Given the constraints from low energy experiments [10] these are studied with the additional simplifying assumptions that:

[2] At high momentum transfer Z^0 and W exchanges become more important and contribute to less pronounced differences between signal and background.

- These are the only sizeable $\not{R}_p$ couplings such that rapid proton decay is avoided and one of these λ'_{ijk} dominates.
- Only couplings to fermions of the first generation are considered.
- Squarks of the first and second generation are degenerate in mass. The case of a light top–squark is considered separately.
- Squarks decay either via their Yukawa couplings into fermions, or via their gauge coupling into a quark and the LSP (fig. 1b) which is assumed to be the lightest neutralino χ_1^0. In this extension of the MSSM, the χ_1^0 decays dominantly into a quark, an antiquark and a lepton. Cascade decays via other gauginos are neglected.

The Yukawa couplings resemble very much the ones for leptoquarks, and the production cross-section for *up*–type squarks is indeed the same as the one of the $\tilde{S}_{1/2}$ leptoquark. The same resemblance holds for *down*–type squarks and the S_0 leptoquark. Also the partial decay width for the $\not{R}_p$ decay into fermions is the same. Under the further simplifying assumption that the neutralino is a pure photino $\tilde{\gamma}$, the gauge decay width is given by

$$\Gamma_{\tilde{q}\to\tilde{\gamma}q} = \Gamma_{\tilde{q}\to eq'}\,\frac{2e^2e_q^2}{\lambda'^2}\,\left(1-\frac{M_{\tilde{\gamma}}^2}{M_{\tilde{q}}^2}\right)^2$$

and contributes mainly at low $\tilde{\gamma}$ masses and low Yukawa couplings. Also in this decay mode an electron or a neutrino is expected together with hadronic activity, so that a common event selection can be used for all signatures. It is however interesting to note that decays also into positrons are predicted, a striking signature for lepton number violation.

Contact Interactions

The search for new bosons can be extended considerably beyond the kinematic limit for their direct production through the study of indirect effects from *virtual* exchange. With particle masses M_X well above the available energy, such indirect signatures may be investigated by adding general contact interaction terms to the SM Lagrangian. For sufficiently heavy particles X the propagator is contracted and new effective four-fermion point-like interactions arise. The separate dependence of amplitudes on M_X and on couplings $g_{X\to i,\,f}$ to initial and final states i, f reduce to the dependence on effective couplings with dimension [mass^{-2}]

$$\eta_{if} \quad\equiv\quad \frac{g_{X\to i}\;g_{X\to f}}{M_X^2}\ .$$

Interference of the new current with the γ and Z fields of the SM may lead to observable effects in neutral current (NC) deep inelastic scattering at energies considerably lower than the relevant mass scale.

The most general chirally invariant NC contact term Lagrangian can be written in the form [11]

$$\begin{aligned}\mathcal{L}^{NC}_{\text{contact}} \quad = \quad & \sum_q \{\eta^q_{LL}\,(\bar{e}_L\gamma_\mu e_L)(\bar{q}_L\gamma^\mu q_L) + \eta^q_{LR}\,(\bar{e}_L\gamma_\mu e_L)(\bar{q}_R\gamma^\mu q_R) \\ & + \eta^q_{RL}\,(\bar{e}_R\gamma_\mu e_R)(\bar{q}_L\gamma^\mu q_L) + \eta^q_{RR}\,(\bar{e}_R\gamma_\mu e_R)(\bar{q}_R\gamma^\mu q_R)\}\ ,\end{aligned}$$

where the indices L and R denote the left-handed and right-handed fermion helicities and the sum extends over *up*–type and *down*–type quarks q. Although contact interactions have been originally proposed in the context of composite quarks and leptons [12, 13], this ansatz can be easily applied to other new phenomena, like leptoquarks, by an appropriate choice of the coupling coefficients η_{if} [11].

3 The H1 detector

A detailed description of the H1 detector can be found in [14]. Here we describe only the components relevant for the present analysis in which the event final state involves a lepton (electron or neutrino) with high transverse energy E_T, balanced by a large amount of hadronic E_T flow.

The electron energy and angle are measured in a finely segmented liquid argon (LAr) sampling calorimeter [15] covering the polar angle[3] range $4^\circ \leq \theta \leq 153^\circ$ and all azimuthal angles. It consists of a lead/argon electromagnetic section, with a thickness varying between 20 and 30 radiation lengths and is composed of three (in the barrel region) to four (in the forward region) layers of cells in depth. This section is followed by a stainless-steel/argon hadronic section for the measurement of hadronic energy flow which offers in total a containment varying from 4.5 up to 8 interaction lengths. The hadronic section has four (barrel) to six (forward) layers of cells in depth. In the LAr calorimeter, electron energies are measured with a resolution of $\sigma(E)/E \simeq 12\ \%/\sqrt{E} \oplus 1\%$ and hadron energies with $\sigma(E)/E \simeq 50\ \%/\sqrt{E} \oplus 2\%$ after software energy weighting [16]. The absolute energy scales are known to 2% and 5% for electrons and hadrons respectively. The angular resolution on the scattered electron measured from the electromagnetic shower in the calorimeter is about 7 mrad. A lead/scintillator electromagnetic backward calorimeter extends the coverage at larger angles ($155^\circ \leq \theta \leq 176^\circ$).

Located inside the calorimeters is the tracking system used here to determine the interaction vertex and the charge of the final state lepton. The main components of this system are central drift and proportional chambers ($25^\circ \leq \theta \leq 155^\circ$), a forward track detector ($7^\circ \leq \theta \leq 25^\circ$) and backward proportional chambers ($155^\circ \leq \theta \leq 175^\circ$). The tracking chambers and calorimeters are surrounded by a superconducting solenoid coil providing a uniform field of 1.15 T within the tracking volume. The instrumented iron return yoke surrounding this coil is used to measure leakage of hadronic showers and to recognize muons. The luminosity is determined from the rate of the Bethe-Heitler process $ep \rightarrow ep\gamma$ measured in a luminosity monitor as described in [14].

4 Event simulation

The Monte Carlo simulation of leptoquarks and leptogluons [17] was performed using the differential cross-sections from [3, 7]. For leptoquarks, the interference with DIS Standard Model amplitudes is treated and leads to significant contributions only at the largest accessible masses and couplings. For squarks decaying into a lepton and a quark, the event generator for leptoquarks could be used since the final states and kinematics are indistinguishable. For squarks undergoing a gauge decay into a quark and a neutralino, a generator [17] based on the cross-sections given in [10] was adopted. Both generators also simulate initial state bremsstrahlung in the Weizsäcker–Williams approximation, initial and final state parton showers and fragmentation [18]. The kinematics at the decay vertex are corrected for effects of the parton shower masses. The parton density used is evaluated at the scale of the new particle mass, and this scale is also chosen for the

[3]The incoming proton moves by definition in the forward (i.e. $z > 0$) direction with $\theta = 0^\circ$ polar angle.

maximum virtuality of parton showers. Systematic effects due to alternative choices will be discussed later.

The SM prediction for DIS is obtained via the event generator [19], which includes the lowest order electroweak scattering process with QCD corrections to first order in α_s, complemented by leading-log parton showers and fragmentation [18]. A comparison with a simulation [20] of DIS events based on a complete first order electroweak corrected cross-section revealed no significant differences for our purposes. Direct and resolved photoproduction events of light and heavy quarks were considered for background studies using the generator [18].

The parton densities in the proton used throughout are taken from the MRS D$-$ [21] parametrization which is close to recent F_2 structure function measurements at HERA [22]. The parton densities in the photon are taken from the GRV–G LO parametrization [23]. The difference in the results obtained using other existing parametrizations will be discussed later.

To compare data and the SM expectation an absolute normalization based on the predicted cross-section and the measured luminosity is applied. All simulated events were passed through a detailed Monte Carlo program of the H1 detector including all acceptances, resolutions and efficiencies and the same reconstruction and analysis programs were used as for data.

5 Analysis methods

5.1 Kinematics

Two mass reconstruction methods are considered, both of which offer good mass resolutions but differ in their systematic behaviour.

Firstly, in the parton model for massless quarks, and assuming that the proton remnant does not participate in the hard interaction, the mass of the leptoquark, leptogluon or squark undergoing two-body decays into $e + q$, $\nu + q$ or $e + g$ can be estimated from the energy available at the hard initial $e + parton$ vertex. It is related to the Bjorken momentum fraction x of the parton in the proton via

$$M^2 = (p_e + xp_p)^2 = xs$$

where p_e and p_p are the electron and proton beam four-momenta, and x is related to the square of the momentum transfer Q^2 and the Bjorken- y variable through $x = \frac{Q^2}{ys}$. Hence, for $e + X$ channels, the mass M_e can be reconstructed from the final state electron energy E_e and angle θ_e as

$$M_e = \sqrt{\frac{Q_e^2}{y_e}}, \quad Q_e^2 = \frac{P_{T,e}^2}{1 - y_e}, \quad y_e = 1 - \frac{E_e - P_{z,e}}{2E_e^0}, \quad P_{T,e} = E_e sin\theta_e$$

for the electron beam energy E_e^0.

For $\nu + X$ channels, all visible final state hadrons are summed over:

$$M_h = \sqrt{\frac{Q_h^2}{y_h}}, \quad Q_h^2 = \frac{P_{T,miss}^2}{1 - y_h}, \quad y_h = \frac{\sum(E - p_z)}{2E_e^0}, \quad P_{T,miss} \equiv \mid \sum \vec{P}_T \mid$$

In these methods, particles which disappear in the beampipe and higher order effects such as initial and final state parton showers and initial state radiation from the electron have influence on the mass reconstruction. Especially important is the virtuality of the final state quark, since it destroys the naïve parton model kinematics at the leptoquark decay vertex. Using x for the mass calculation means that we rely on the Monte Carlo simulation to provide an accurate description of these effects.

As an alternative method, the mass of the resonance can be computed as the invariant mass M_{dec} of all final state decay products. It requires the removal of the hadronic energy flow associated with fragments of the proton. This is done via a cut in pseudorapidity, $\eta_{cut} = \eta_h + 1.5$. Here η_h is the pseudorapidity of the jet with the highest transverse energy among the jets found by a cone algorithm with cone opening angle R=1 in units of pseudorapidity and azimuthal angle. The mass is then computed from the sum, restricted to the angular range $\theta > 10°$, of all particles with $\eta < \eta_{cut}$. This method is largely independent of the higher order effects mentioned above. It can also be used for gauge decays of squarks into multi-particle final states.

The two reconstruction methods are compared in fig. 2 for simulated events. For DIS

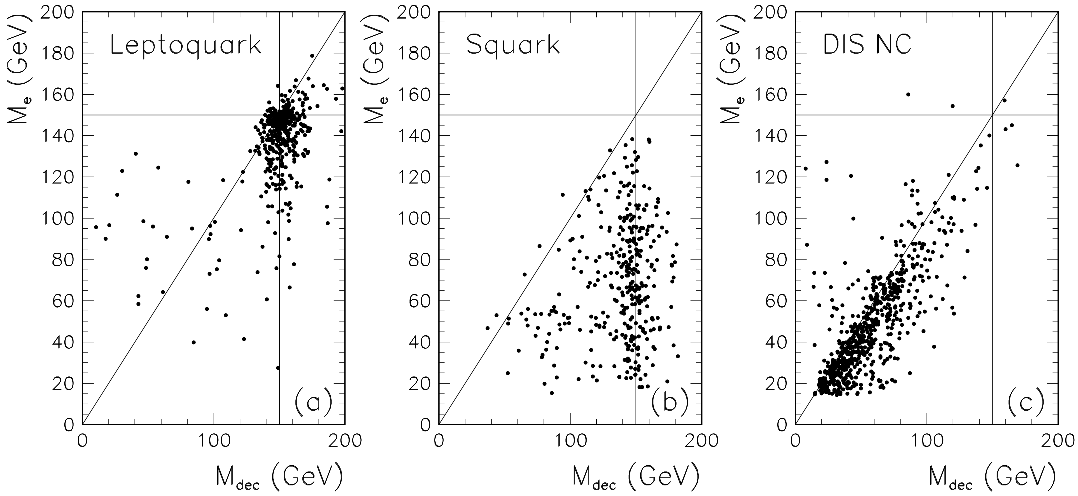

Figure 2: *Reconstructed masses M_e from the electron versus M_{dec} from the decay products for a simulation of (a) scalar leptoquarks and (b) gauge decay of squarks at masses of* 150 GeV*; (c) Similar correlation plot for Standard DIS NC events.*

Neutral Current events (fig. 2c) the correlation between the two methods is very good. The tail towards larger M_{dec} values originates from events where too much energy from the proton remnant is collected.

For leptoquarks (fig. 2a), the mass is also well reconstructed by both methods and peaked at the generated mass value with FWHM resolutions of 8 and 14 GeV for M_e and M_{dec} respectively. The tail towards higher M_{dec} values appears here as well. The events migrating towards low M_e originate from small y where the higher order effects (especially the off-shellness of the final state quark) become important. Since a rather high scale for the final state parton shower was used, the relatively few events in this tail demonstrates that such systematic effects are not too severe for the M_e method. M_{dec} is also sometimes found to be underestimate at low y_e where the jet associated to the final state quark in the leptoquark decay is at low angles and partly truncated by the forward angular cut mentioned above. These low y events will be suppressed later by cuts on y_e used to separate a possible signal from the DIS background.

For gauge decays of squarks however (fig. 2b), only M_{dec} correctly estimates the generated mass since the calculation via M_e assumed, improperly here, a two-body decay into massless particles. This difference will be used later to distinguish the decay $\tilde{q} \rightarrow q\chi_1^0$ from the DIS background.

In view of the tails towards higher masses in the expected DIS background sample for the M_{dec} method, we will use M_e to analyse leptoquark and squark decays into $e + jet$, and M_{dec} only for gauge decays of squarks. The χ_1^0 mass is computed in the same way as M_{dec} but excluding a region of $\pm 45°$ in azimuthal angle around the axis of the highest E_T jet.

5.2 Event selection

The event selection is common to all $e + X$ final states or to all $\nu + X$ final states and consists essentially of electron finding algorithms and global energy conservation cuts.

Event candidates for $e + X$ final states must satisfy the following requirements:

1. a primary vertex must be reconstructed in the range $\mid z - \bar{z} \mid < 35$ cm with $\bar{z} = -5.0$ cm;
2. an electron satisfying $E_{T,e} > 7$ GeV and $10° \leq \theta_e \leq 145°$ has to be found in the LAr calorimeter;
3. the total missing transverse momentum $P_{T,miss} \equiv \mid \sum \vec{P}_T \mid \approx \sqrt{(\sum E_x)^2 + (\sum E_y)^2}$ measured by the calorimeters must satisfy $P_{T,miss} \leq 15$ GeV, where the sums run over all energy depositions in the calorimeters;
4. the energy-momentum conservation requirement $\mid \sum(E - p_z) - 2E_e^0 \mid \leq 10$ GeV must be satisfied, where E_e^0 is the incident electron energy;
5. the total energies E_{back} in the backward calorimeter and E_{tag} in the electron tagger of the luminosity monitor must satisfy $E_{back} < 10$ GeV and $E_{tag} < 5$ GeV;
6. the scaling variable y_e must fulfil $0.05 < y_e < 0.95$.

The requirements (1), (2) and (3) suppress beam–wall or beam–residual gas induced background as well as background from cosmic rays and DIS charged current (CC) events. Cut (4) provides powerful rejection of events with energy losses in the beam pipe along the incident electron direction. This suppresses events with a very hard γ emitted from the electron in the initial state and, together with cut (5), photoproduction contamination with a misidentified electron in the LAr calorimeter. Cut (5) also eliminates contamination from DIS events at small momentum transfer with misidentified electrons. Cut (6) rejects the high y_e region to avoid the largest radiative corrections and to further suppress the photoproduction background. It also rejects the low y_e region where the y_e and M_e resolutions severely degrade.

The electron identification essentially relies on shower estimators similar to those described in [24]. We require that 90% of the electron energy be contained within the electromagnetic section and that the fraction deposited in the first layer exceeds a fixed threshold parametrized according to polar angle. Moreover, cuts on the transverse shower moments are applied. Finally, we impose a weak electron isolation criterion : the electron shower must possess 90% of the energy integrated in a cone centered on the electron pseudorapidity η_e and azimuth ϕ_e of opening $\sqrt{(\Delta\eta_e)^2 + (\Delta\phi_e)^2} < R$ where R=0.25. Also there should be no muon track and no instrumented iron cell firing behind the electron in a cylinder of fixed radius centered on the electron axis.

Event candidates in searches for the $\nu + X$ final state must satisfy the following requirements developed for the deep inelastic charged current analysis [25] at high Q^2:

1. a primary vertex must be reconstructed in the range $\mid z - \bar{z} \mid < 35$ cm with $\bar{z} = -5.0$ cm;
2. no electron satisfying the requirements of the $e + X$ selection should have been found;
3. the total missing transverse momentum measured by the calorimeters must satisfy $P_{T,miss} > 15$ GeV;
4. the total transverse energy $E_T \approx \sum \mid \vec{P}_T \mid$ should match the total missing transverse momentum $P_{T,miss}$ such that $(E_T - P_{T,miss})/E_T < 0.5$;
5. the event must survive a set of halo and cosmic muon filters described in [25]; residual superimposed events are removed by a visual scan;
6. the scaling variable y_h as measured from the final state hadronic energy flow must satisfy the cut $y_h < 0.95$.

The requirements (1) and (5) suppress halo muons produced upstream by the proton beam as well as background from cosmic rays. The requirements (3) and (4) strongly suppress proton–wall and proton–residual gas collisions as well as photoproduction and taken together with (2) they reject deep inelastic neutral current contamination; all these backgrounds generally lead to events balanced in transverse momenta.

In addition, for both $e + X$ and $\nu + X$ channels, events perturbed by well understood and easily recognized coherent noise patterns in the LAr calorimeter were rejected. The events must have been accepted by LAr hardware triggers which use energy summed in coarsely segmented calorimeter trigger readout. For the $e + X$ channels, we require that either the total electromagnetic energy in a narrow tower *or* the total barrel energy *or* the total transverse energy exceed fixed thresholds. For the $\nu + X$ channels, a vector sum of transverse momenta has to exceed a fixed threshold. All LAr trigger thresholds were set just above the electronic noise.

With the above selection requirements, we are left at this point with a sample of 784 events in the $e + X$ channels. As will be shown in section 5.3, the above selection requirements are most efficient in the mass range > 45 GeV. We find 485 events with either $M_e > 45$ GeV or $M_{dec} > 45$ GeV. Out of these, about 65% have $M_e > 45$ GeV and 92% have $M_{dec} > 45$ GeV. In the $\nu + X$ channel, 13 events are found with masses $M_h > 45$ GeV.

Additional or more stringent requirements are imposed for the decay $\tilde{q} \rightarrow \chi_1^0 + q$ where the χ_1^0 balances in transverse momenta the opposite jet which acts in the final state like the "current jet" in DIS. The χ_1^0 then decays to $e + 2jets$. In the mass range considered in this paper ($M_{\chi_1^0} \gtrsim 10$ GeV), the electron is generally isolated enough to satisfy the selection requirements but nevertheless lies within $\pm\pi/2$ in azimuth of the hadronic energy flow from the decay jets. Hence we require the transverse hadronic energy flow in this ϕ range around the electron to be at least 10% of that of the "current jet". Moreover, the y_e distribution for such squark decays appears strongly shifted towards large y_e. This is because the scalar squark decays uniformly in its center-of-mass frame (as a scalar leptoquark which has a flat y_e distribution) but only part of the χ_1^0 energy goes to the final state electron. Hence we require that $y_e > 0.4$ independently of the $\tilde{q}$ or χ_1^0 masses. Finally, M_{dec} is required to deviate from M_e by more than 10% as a complementary and powerful cut against DIS NC background (see fig. 2b and c).

We find 60 candidates satisfying the cuts specific to gauge decays of squarks, and with masses $M_{dec} > 45$ GeV.

5.3 Efficiencies and background contamination

The signal efficiencies estimated from Monte Carlo simulation by applying the selection criteria described in section 5.2 are shown in fig. 3a and c for leptoquarks (or squarks decaying via $\not{R}_p$ coupling) and 3d for leptogluons. In order to take into account properly effects from the intrinsic width of the resonance, the coupling for each type of particle or decay was chosen to correspond to a cross-section at the expected limit of sensitivity. The selection efficiency is found in all cases to be of order $80 - 90\%$ in the mass range $75 \lesssim M \lesssim 200$ GeV. For leptoquarks, the efficiency is seen to drop at masses $M \gtrsim 150$ GeV and $M \gtrsim 250$ GeV for particles carrying the quantum numbers of antiquarks or quarks respectively. In the relevant range of couplings, the decay width is typically smaller than the experimental mass resolution. Only at high masses and correspondingly high couplings does the width become broad. Together with the steeply falling quark density function, this leads to distributions with long tails towards lower masses. Given the systematic uncertainties on the shape of the parton densities we cut off this tail, which leads to the reduced efficiency at very high masses.

The selection efficiency also severely drops below $M \lesssim 50$ GeV owing to the $E_{T,e}$ and θ_e requirements for the final state electron. In the following sections, all results are presented in the restricted mass range $M > 45$ GeV.

The remaining contamination from photoproduction events was estimated by Monte Carlo. The upper limits were found to be $< 0.6\%$ from $\gamma + p \rightarrow jet + jet$ (direct and resolved photon processes) and $< 0.5\%$ from heavy flavour pair production by boson–gluon fusion processes. These numbers are consistent with the absence of selected events with an electron tagged in the luminosity detector.

Single non-colliding electron or proton bunches were used to monitor the contamination due to interactions which do not origin from ep collisions. No such event survived the selection cuts.

For squarks undergoing gauge decays into $\chi_1^0 + jet$ where the χ_1^0 decays into $e + 2jets$, the efficiency (see fig. 3b) depends on the neutralino mass and is found by Monte Carlo simulation to reach up to 70% at the higher χ_0^1 masses.

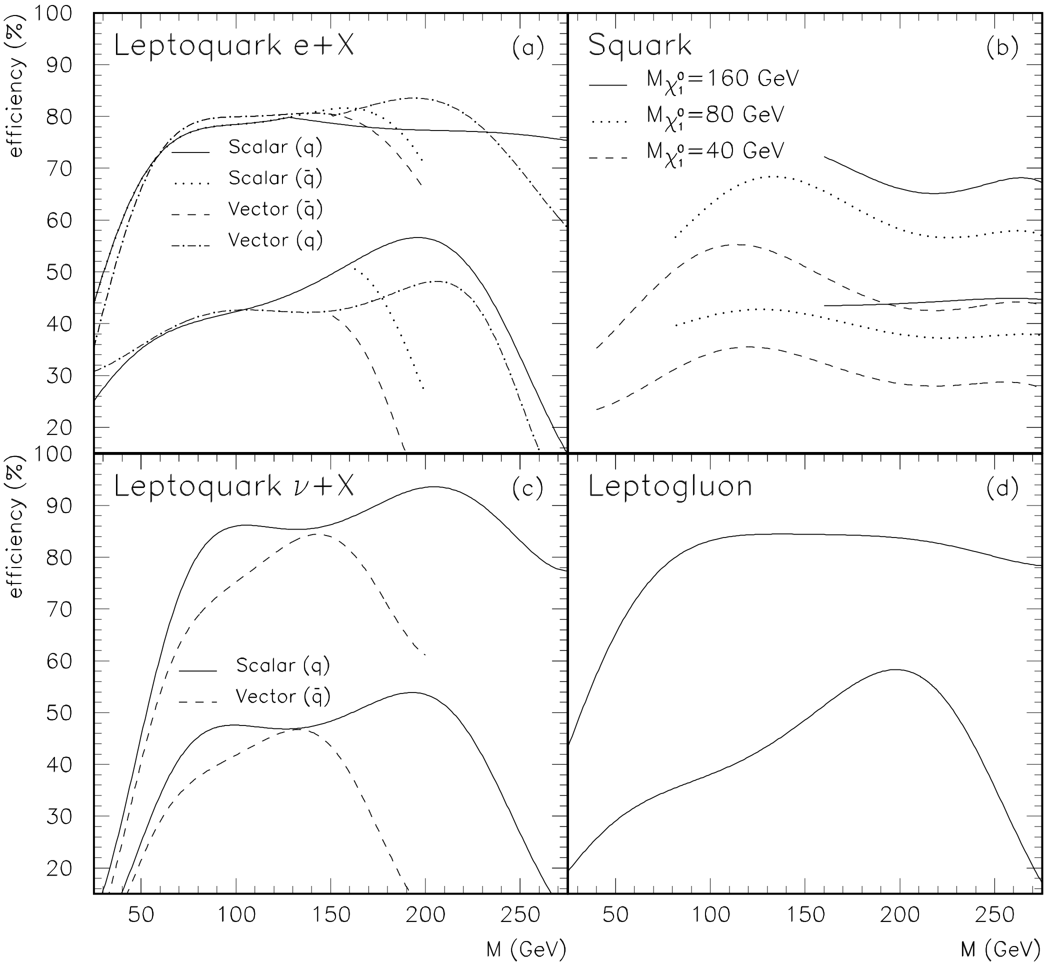

Figure 3: *Selection efficiencies for (a) leptoquarks in the $e+q$ channel, (b) squarks in the $q+\chi_1^0$ decay mode, (c) leptoquarks in the $\nu+X$ channel and (d) leptogluons. For every case considered, the curves with higher efficiencies correspond to the basic selection, while the lower curves give the actual efficiency remaining after applying mass and y windows (section 6) to optimize the signal to background ratio.*

6 Direct search for leptoquarks and leptogluons

We first compare our $e+X$ and $\nu+X$ sample with predictions from the Monte Carlo simulation of Standard Model DIS events. Figures 4a and 4c show the measured $e+X$ data and the corresponding Monte Carlo distribution in the y_e versus M_e plane. The DIS simulation shown here was obtained from a sample equivalent to 3 times the data luminosity and exhibits the expected increase of the cross-section towards lower y_e values and lower masses, and agrees well in shape with the measured data. The cut off at low y_e and low mass is due to the minimum transverse momentum requirement mentioned before. Overlayed on the DIS expectation are some simulated events from a scalar leptoquark of 200 GeV.

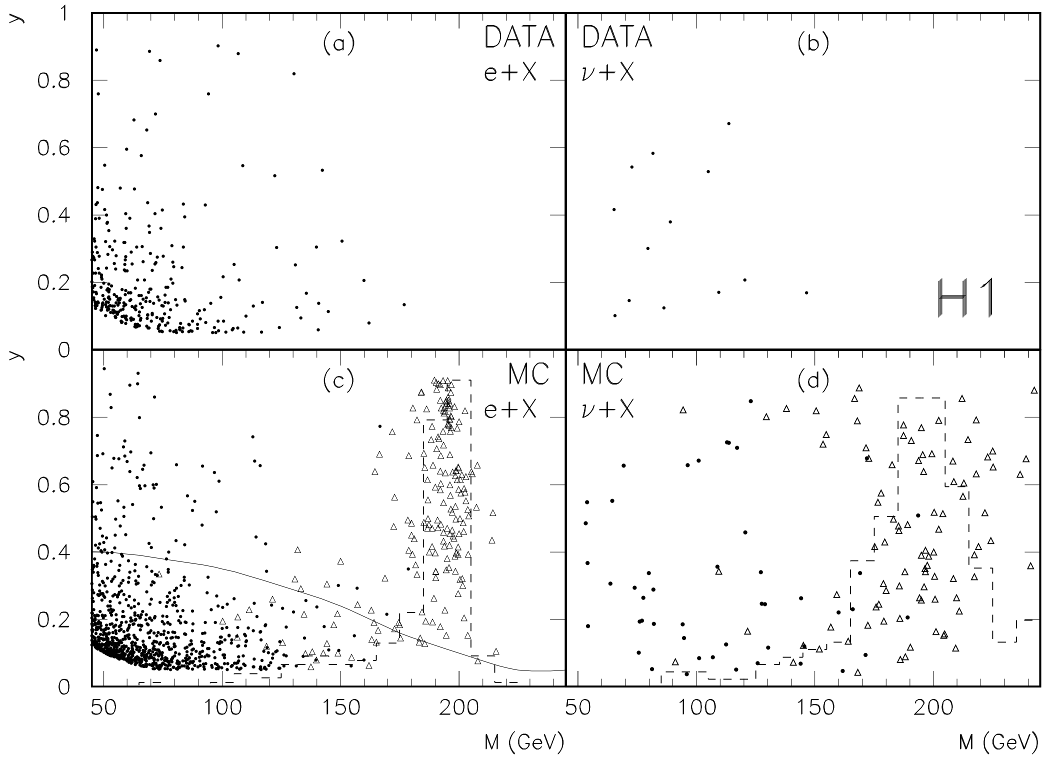

Figure 4: *(a) and (c) y_e versus M_e for $e + X$ final states; (b) and (d) y_h versus M_h for $\nu + X$ final states. The data are shown in (a) and (b). In (c) and (d) are DIS Monte Carlo events (dots) superimposed with a scalar leptoquark (triangles) at $M = 200$ GeV and $\lambda = 0.25$. The dashed histograms are the mass projections for this leptoquark illustrating the mass resolutions. The curve in (c) shows the mass dependent y_e cut used to optimize the sensitivity to new scalar particles.*

Figures 4b and 4d show the corresponding $\nu + X$ distributions, where now only the hadronic final state is available to determine the kinematics. Here also the DIS CC Monte Carlo sample corresponds to 3 times the integrated luminosity for the measured $\nu + X$ sample. Again the shape of the data is well reproduced by the prediction for W- exchange. The mass resolution for a leptoquark however is considerably worse here compared to the $e + X$ case due to the hadronic energy resolution.

The comparison of the measured data and DIS Monte Carlo predictions are shown in the mass spectra of fig. 5a for $e + X$ and fig. 5b for $\nu + X$ data. Here we make use of the full DIS Monte Carlo sample which amounts for NC (CC) to 6.2 (130) times the measured luminosity. For $e+X$ data, the mass spectrum is shown before and after having applied a mass-dependent y_e cut (see curve in fig. 4c) designed to optimize the signal over background significance for scalar leptoquark searches; this y_e cut will be used later in the derivation of rejection limits. For $\nu + X$ data, no equivalent cut is applied since the expected CC background does not concentrate at low y. Before the y_e cut, both mass spectra are found to be well described by the SM Monte Carlo over the full mass range above 45 GeV. We observe 314 $e + X$ events in this mass range while 298 ± 7 events are

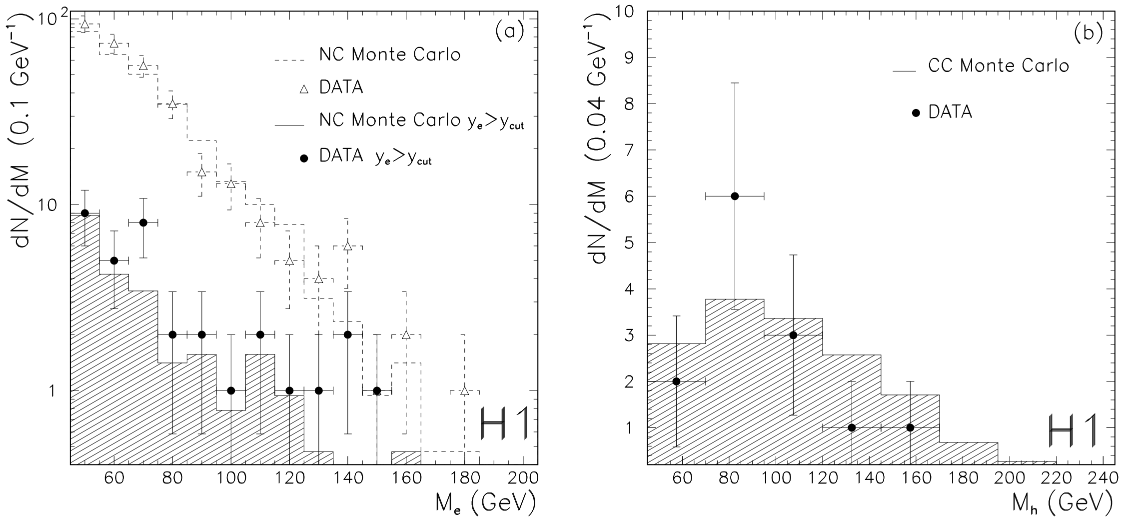

Figure 5: *Mass spectra for $e + X$ (a) and $\nu + X$ (b) final states for data (closed points) and DIS Monte Carlo (shaded histograms). Also shown in (a) is the data (open triangles) and DIS NC Monte Carlo (dashed histogram) compared before the final y_e cut (see text).*

expected. In the $\nu + X$ channel, we expect 15.3 ± 0.3 events compared to the observed 13 events. Also after the y_e cut, the shape of the remaining $e + X$ data in fig. 5a is well described by Monte Carlo but an excess of events in this high Q^2 region at large y_e is observed. The 34 measured events represent a 2σ fluctuation above the expected average background of 25.1 ± 2 events. Similar excess is observed if using M_{dec} instead of M_e.

In order to quantify the agreement between the measured data and the SM prediction, and to investigate how eventual deviations could be accounted for by a leptoquark signal, we performed a maximum likelihood analysis exploiting the expected shape of the mass and angular (i.e. y) distributions. The likelihood is calculated as $\mathcal{L} = \Pi_{i=1}^{N} \mathcal{P}(M_i, y_i, M_{LQ}, \lambda)$ where $\mathcal{P}(...)$ is the probability to obtain an event i measured with kinematic values (M_i, y_i) in the hypothesis that a leptoquark with mass M_{LQ} and coupling λ sits on top of the standard DIS NC contribution, i.e.

$$\mathcal{P}(M_i, y_i, M_{LQ}, \lambda) = 1/\mathcal{N}(\lambda) \left[\frac{d^2\sigma^{NC}}{dMdy}(M_i, y_i) + \frac{d^2\sigma^{LQ}}{dMdy}(M_i, y_i) \right]$$

The normalization $\mathcal{N}(\lambda)$ is chosen such that we attribute any overall excess to systematic errors in the total DIS NC cross-section so that the sum of the integrated DIS and leptoquark distributions corresponds to the total number of measured events. The effects of interference between standard DIS processes and leptoquark boson exchange are negligible in the mass range spanned by the actual data[4]. Increase of the likelihood in the leptoquark hypothesis relative to the no signal hypothesis (i.e. $\lambda = 0$) are observed at the 2 to 3σ level within the 65 to 80 GeV range and within the 125 to 150 GeV range. The probability to observe in a single measurement a deviation of more than $+2\sigma$ arising from

[4]Note that constructive and destructive contributions of the interference below and above the leptoquark mass pole partially cancel.

purely statistical background fluctuations somewhere in the coupling-mass plane considered is 40%. For vector leptoquarks the deviations are smaller indicating that the excess of events mainly occurs at high y.

Having observed no significant deviations from the expectations of the Standard Model, we calculate the most probable rejection limits at 95% confidence level (CL) for a single leptoquark at fixed mass (cf. fig. 6).

Scans of the mass spectra are carried out in 1 GeV steps. The signal efficiency, the number of observed events and the number of expected background events are integrated within a mass bin. For the $e+X$ channel, the y_e cut mentioned before is applied for each mass hypothesis. The width of the mass bin and the y_e cut are tuned independently to optimize the signal significance assuming an experiment where the number of observed events would correspond exactly to the mean expected number of background events. The corresponding efficiencies are given in fig. 3a and 3c.

Whenever relevant, decay modes are combined with branching ratios fixed by the model described in section 2. In this case the calculation of the rejection limit makes use of the product of the Poisson probabilities $\mathcal{P}(N_k, \epsilon_k S + b_k)$ where each channel k enters with an efficiency ϵ_k (= reconstruction efficiency $\times$ branching ratio), N_k observed events and b_k mean expected background events, to detect a signal S given the measured luminosity.

Integrating this probability up to 95% of the total integral yields the upper limit for the signal, from which we calculate the upper limit of the coupling constant λ. For a single decay channel this is identical to the prescription given by the particle data group [26].

We furthermore take into account statistical and systematic errors in the contribution of the efficiencies ϵ_k and backgrounds b_k.

- The error of the luminosity measurement is 5%.
- The statistical uncertainty on the reconstruction efficiency is $\leq 4\%$.
- The statistical error of the background estimate is negligible at low masses, and ranges up to 30 % at high masses.
- The absolute energy calibration for electrons (2%) and hadrons (5%) results in an uncertainty on the background estimation of 10%.
- The scale entering the structure function calculation leads to uncertainties in the cross-section of $\approx 7\%$.
- The error on the efficiency loss due to the vertex cut is below 1%.

For the error on the luminosity, a Gaussian smearing is applied in common for all contributing decay channels. All other uncertainties are propagated by folding Gaussian distributions for ϵ_k or b_k into the integral mentioned above. The statistical and systematic errors weaken the coupling limits by about 4%.

The resulting exclusion limits are shown in fig. 6 for leptoquarks and fig. 7 for leptogluons. The curves have been smoothed taking into account the finite mass resolution. Using other recent parton density parametrizations (MRS D0 [21], GRV HO [27], MT B2 [28]) would yield differences of typically less than 5% at low masses and 20% at the highest masses.

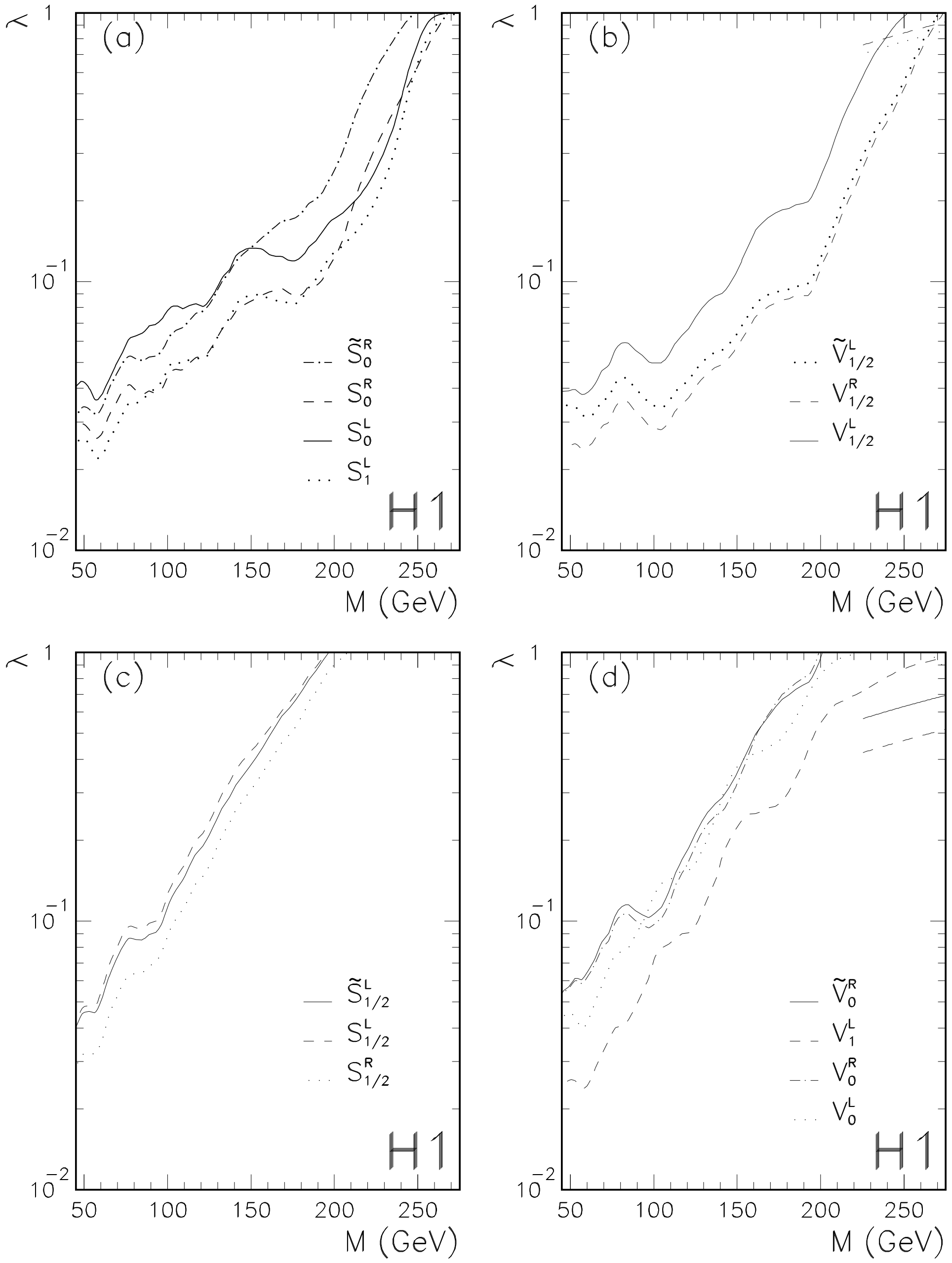

Figure 6: *Upper limits at 95% CL as a function of mass on the coupling* $\lambda_{L,R}$ *for scalar and vector leptoquarks decaying into lepton+q (a,b) and lepton+*$\bar{q}$ *(c,d). The limits on* λ_L *for* S_0, S_1, V_0 *and* V_1 *combine* $e+X$ *and* $\nu+X$ *decays. The additional lines at high masses in (b) and (d) represent the result of the indirect search via the contact term analysis.*

For small masses, where the quark densities are high, very small couplings are accessible with the present luminosity, while at masses close to the kinematic limit $\sqrt{s}$, the quark densities become so low that couplings of the order $\lambda \approx 1$ are necessary to obtain observable cross-sections. There, the contribution of interference is sizeable for vector

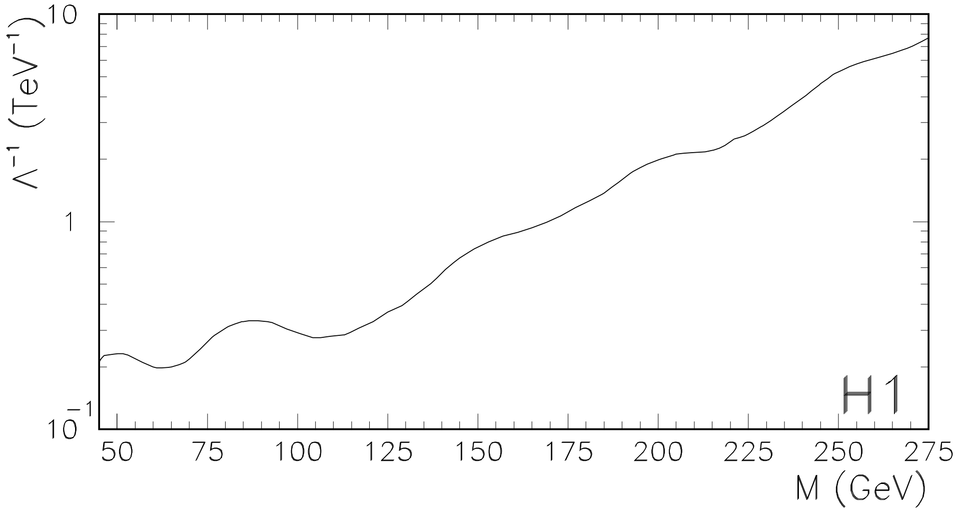

Figure 7: *Upper limit at 95% CL for the inverse of the scale parameter* Λ *versus* M *for leptogluons.*

leptoquarks. As expected the limits are lower for leptoquarks coupling to quarks than for those coupling to antiquarks. With the present luminosity masses up to 270 GeV can be excluded, and couplings one order of magnitude weaker than the electromagnetic coupling ($\lambda = 0.3$) are accessible. For couplings of electromagnetic strength, leptoquarks are restricted to be heavier than 130 to 230 GeV depending on the leptoquark quantum numbers.

Direct searches for leptoquarks have been carried out also at the Tevatron $p\bar{p}$ collider [29]. Since there leptoquarks are produced mainly via a virtual gluon, these limits are independent of the coupling λ to electron–quark pairs, but for vector leptoquarks depend on assumptions of the size of the anomalous coupling to gluons. The most stringent *model independent* searches [29] are presently restricted to scalar leptoquarks with masses below 120 (133) GeV and to vector leptoquarks with masses below 189 (195) GeV with branching ratio 0.5 (1) into electron and quark. Indirect limits from low energy experiments will be discussed in the following section.

For leptogluons we exclude (fig. 7) compositeness scales of 3 TeV at masses of 100 GeV and masses below 240 GeV are forbidden for scales of 250 GeV. In comparison, masses below 110 GeV have been excluded from $p\bar{p}$ collider data [30].

7 Results from contact terms analysis

The analysis is based on a purely inclusive measurement of the Q^2 spectrum measured with the final state electron. The $e + X$ sample described in section 5.2 is restricted explicitly to $E_{T,e} > 10$ GeV and $y_e < 0.8$ in order to avoid the region affected by the largest radiative corrections. This leads to a reduced data sample of 691 events. For the SM prediction, we use the Monte Carlo simulation described earlier. The contact term contributions are derived by re-weighting the SM Monte Carlo events with the appropriate lowest order cross-section for a particular choice of couplings η_{if}. Any deviation from the SM prediction for DIS NC events will be interpreted in terms of contact interactions.

Figure 8 shows the measured Q^2 distribution compared to the SM prediction. We observe no significant deviation as the data is well described by the simulation over two decades in event density. This also holds for high Q^2 where the largest contribution from a contact interaction is expected. This is demonstrated in fig. 8 via the example of the allowed contribution (95% CL) from the leptoquark V_1^L. This distribution looks very

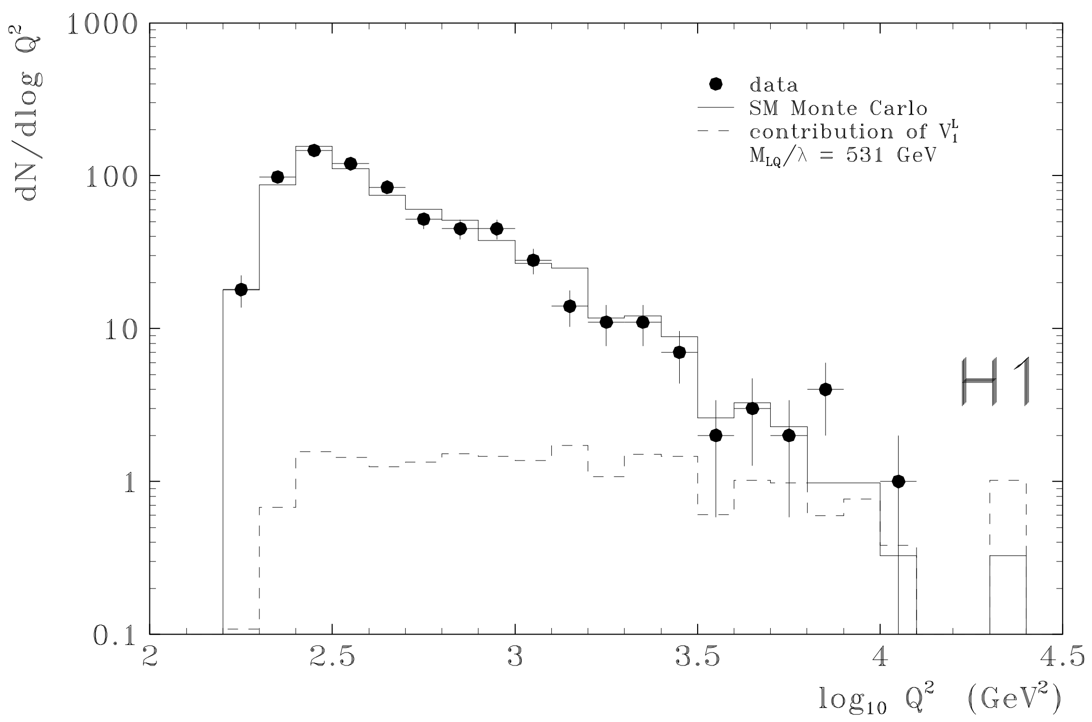

Figure 8: *Measured* $\log Q^2$ *event distribution. The data (•) are compared to the Standard Model prediction (—) and to the allowed contribution (95% CL) of an additional leptoquark (−−). The leptoquark type is* V_1^L *with coupling* $M_{LQ}/\lambda = 531$ GeV.

different from the data, it is rather flat and exhibits comparable contributions to the SM only at the highest Q^2 values.

To calculate limits on a possible leptoquark contribution, a χ^2 analysis [11] is performed allowing for a normalization within the systematic error of $\Delta_{sys} = 5\%$. Lower limits (95% CL) on the four coupling coefficients η_{if} are derived from the fits at $\chi^2(\eta_{if}) = \chi^2_{min} + 4$. The resulting limits on M_{LQ}/λ are summarized in the last column of table 1. Only the four leptoquarks with the highest coupling to up-type quarks are mentioned since only they give limits reaching or exceeding the kinematic limit of HERA for $\lambda \sim 1$.

LQ type	coupling to u quarks	coupling to d quarks	M_{LQ}/λ $[GeV]$
$\tilde{V}_0^R$	$\eta_{RR}^u = +\lambda^2/M_{LQ}^2$		397
$V_{1/2}^R$	$\eta_{RL}^u = +\lambda^2/M_{LQ}^2$	$\eta_{RL}^d = +\lambda^2/M_{LQ}^2$	297
$\tilde{V}_{1/2}^L$	$\eta_{LR}^u = +\lambda^2/M_{LQ}^2$		320
V_1^L	$\eta_{LL}^u = +2\,\lambda^2/M_{LQ}^2$	$\eta_{LL}^d = +\lambda^2/M_{LQ}^2$	531

Table 1: *Contact interaction coefficients η_{if} and 95% CL lower limits on M_{LQ}/λ for vector leptoquark models.*

The contact interaction ansatz assumes that the leptoquark mass is larger than the available cms energy at the hard interaction vertex. De facto the data cover a mass range up to a maximum value of ~ 180 GeV. This means that the indirect limits may be valid for $M_{LQ} \gtrsim 200$ GeV, thus giving access to coupling constants λ of $\mathcal{O}(0.4)$. The effect of the leptoquark propagator on the coupling limits close to the kinematic threshold is estimated to be less than 10%. The results of the indirect leptoquark limits are displayed in the $\lambda - M_{LQ}$ plane of fig. 6 together with the limits from the direct searches. Choosing different structure functions MRS H, MRS D−' or MRS D0' [31] for the calculation of the event weights gives variations in M_{LQ}/λ by less than 5 GeV. Increasing the systematic error to $\Delta_{sys} = 7\%$ would lower the limits by only $\sim 2\%$.

Thus the *indirect* limits derived from virtual leptoquark exchange nicely complement the *direct* searches and partly exceed the kinematic range of HERA at large coupling.

The limits obtained here may be compared to those from other indirect searches for leptoquarks [5]. From atomic parity violation and universality in leptonic pion decays limits in M_{LQ}/λ have been derived of order 2000 GeV to 4900 GeV depending on the leptoquark species. Only at masses above 800 GeV do the limits from flavour changing neutral current start to become more restrictive. These bounds are stronger than the ones derived here, but this measurement provides useful additional information since it is performed at a completely different energy scale.

The Q^2 spectrum is then analysed, in an analogous way as for the leptoquarks, in terms of compositeness searches. HERA offers through contact terms a sensitivity to a compositeness scale Λ where new interactions should arise if quarks and leptons are composite objects having common constituents. The coupling coefficients are now defined as $\eta_{if} = \pm g^2/\Lambda_\pm^2$, where the coupling strength g is conventionally set to $g^2/4\,\pi = 1$. The two signs allow for positive and negative interference with the SM currents. In the present analysis the couplings are restricted to the pure chirality states *LL, LR, RL* and *RR* for both *up* and *down* quarks, i.e. only one coefficient η_{if} per quark flavour is allowed at the time and all others are set to zero.

The results for lower limits of the scale $\Lambda_\pm$ are found to be almost independent of the chiral structure. We obtain at 95% confidence level that $\Lambda_+ > 1.05$ TeV and $\Lambda_- > 0.71$ TeV for both LR or RL chiral couplings, and $\Lambda_+ > 1.25$ TeV and $\Lambda_- > 0.75$ TeV for both LL or RR couplings. Similar studies at e^+e^- and $p\bar{p}$ colliders [26] yield limits which are roughly a factor of 2 to 3 higher.

8 Results for squarks in R-parity violating SUSY

For the gauge decay of squarks, $\tilde{q} \to \chi_1^0 q$, $\chi_1^0 \to e^\pm q\bar{q}$, the reconstructed χ_1^0 mass versus $\tilde{q}$ mass for the 60 data events satisfying the requirements of section 5.2 are shown in fig. 9a. A similar correlation plot is shown for DIS NC Monte Carlo events in fig. 9b. Both the apparent χ_1^0 and $\tilde{q}$ mass distributions and their correlations are well reproduced. For

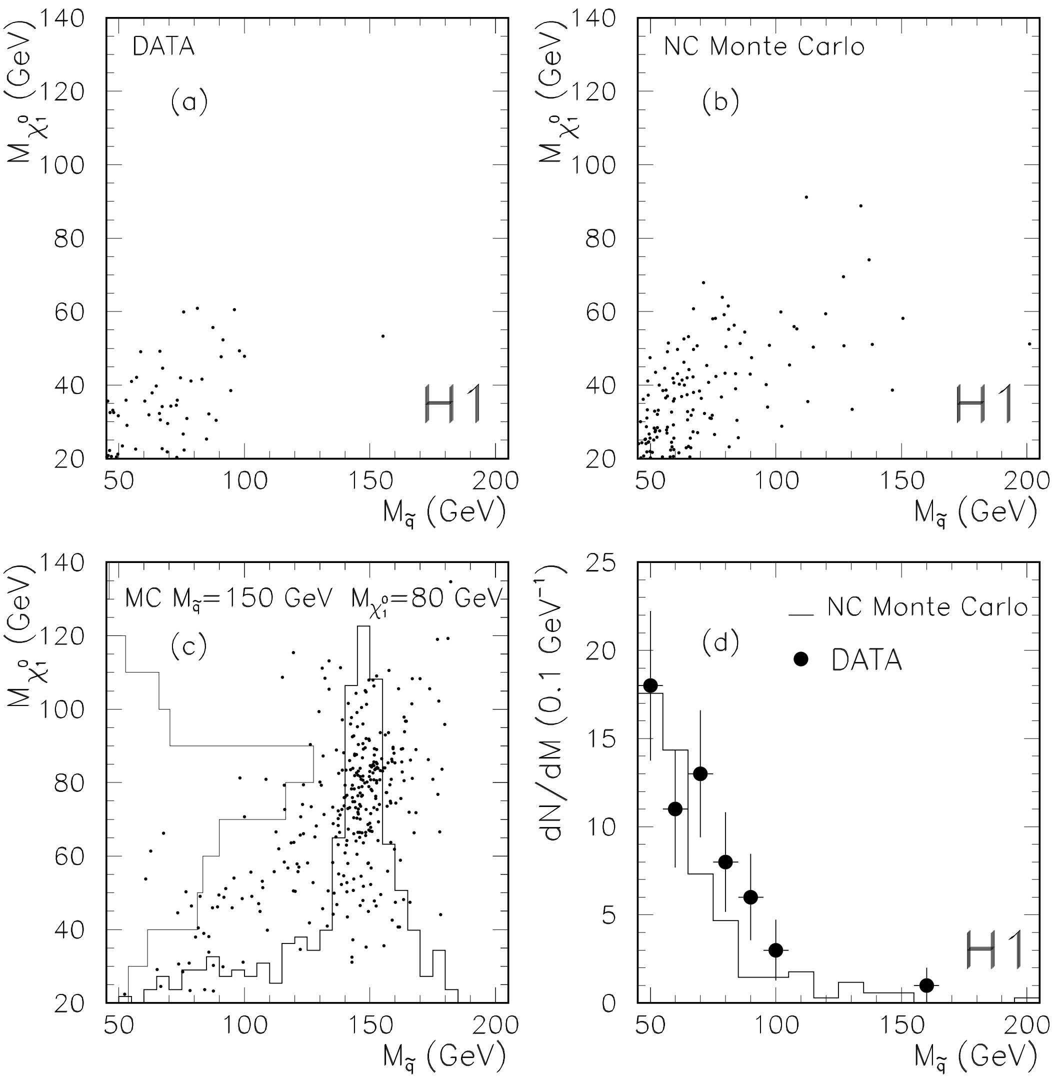

Figure 9: *Apparent neutralino mass versus squark mass for the data (a) and for DIS NC Monte Carlo (b). Typical expectations for squarks undergoing a cascade of decays into $e^\pm + 3jets$ are shown in (c) for $m_{\tilde{q}} = 150$ GeV and $m_{\chi_1^0} = 80$ GeV. (d) Mass spectrum for $e + 3jet$ analysis for data (dots) and DIS NC Monte Carlo (histogram). Figure (c) also shows the mass resolutions for the squark and the neutralino as projections.*

comparison, fig. 9c shows the corresponding Monte Carlo distribution for a $\tilde{q}$ of 150 GeV and a χ_1^0 of 80 GeV. The measured squark mass spectrum (irrespective of the χ_1^0 mass) is shown in fig. 9d. A number of 48 ± 3 background events is expected for $M_{dec} > 45$ GeV. This is in reasonable agreement with observation but for a slight excess (within 1.5 to 2σ from the expected background) spread over a large mass domain. This is not significant in view of the steeply falling mass spectrum and the 5% systematic uncertainty of the hadronic energy scale. Only two events have $M_{\tilde{q}} \geq 100$ GeV while 4 ± 1 are expected. An average of 0.5 ± 0.4 is expected above 150 GeV where one event is found at 155 GeV.

The measured sample considered for the gauge decay modes of the squark has a 20% overlap with the one considered for the $\not{R}_p$ decay modes. This is not surprising since no explicit multi-jet tagging was imposed. As a conservative approach, the shared background will be allowed to contribute (mostly in different mass bins) to both the $\not{R}_p$ and the gauge decay in the derivation of rejection limits.

As was mentioned in section 2, we expect an e^+ in 50% of the $e + 3jets$ final states. Such an explicitly observable violation of lepton number conservation makes it an almost background free channel for squark searches at HERA. Hence for the 60 $\tilde{q}$ candidates we determine the lepton charge from the curvature of the track associated to the electron shower. The event selection was based up to now on calorimetric energy flow quantities only with no direct quality requirements on tracks and no strong requirements on the tracking chamber status. For the shower–track link, it is required that a track extrapolated from the inner surface of the LAr calorimeter passes through the shower volume and that the shower energy E and track momenta P agree within $\mid ((E-P)/(E+P) \mid < 0.5$. Moreover the error in the curvature κ is required to fulfil $1 <\mid \kappa/\delta\kappa \mid < 50$. A fraction of $86 \pm 4\%$ of the showers are thus linked to a charged track. This efficiency compares very well with a value of $87.3 \pm 1.2\%$ obtained for the electrons for the full selection sample of 784 events. From this latter sample we estimate for the $\tilde{q}$ candidates an upper limit of $\sim 3\% \pm 0.6\%$ for mistaking an e^- as an e^+. No such e^+ event is found in the data confirming that the $\tilde{q}$ contribution in fig. 9d can only be small.

In absence of a significant deviation from the SM prediction rejection limits on λ'_{111} are derived for squarks (fig. 10). The calculation follows the prescription of section 6 and combines all decay channels $e + X$, $\nu + X$, $q + \chi_1^0$. To be explicit we assume for the branching ratio calculation that the χ_1^0 is a pure photino $\tilde{\gamma}$ (cf. section 2). The $\tilde{\gamma}$ branching ratio into $e^{\pm}q\bar{q}$ is $\approx 88\%$ [10]. The splitting of the $q + \tilde{\gamma}$ channel into e^+ and e^- involves no efficiency loss, because all events not satisfying the e^+ requirements are accepted in the e^- class. It is further required that the reconstructed photino mass is ≥ 10 GeV (20 GeV) for a true photino mass of $M_{\tilde{\gamma}} = 20, 40$ GeV ($80, 160$ GeV). Using a mass bin optimization method as described in section 6, we obtain efficiencies as shown in fig. 3b. Statistical and systematic errors for the $e + 3jets$ case are similar to those for the leptoquark analysis (see section 6).

For the $\not{R}_p$ decay modes $e+X$, $\nu+X$ the results from the analysis of scalar leptoquarks are used making the replacement that $\tilde{d} \sim S_0$ and $\bar{\tilde{u}} \sim \tilde{S}_{1/2}$. Hence in such modes the squarks are detected with the efficiencies of scalar leptoquarks shown in fig. 3a and the search is made using the mass spectra shown in fig. 5.

The resulting rejection limits are shown in fig. 10, where the $M_{\tilde{\gamma}}$ dependence enters via the acceptance and the available phase space. The limits for λ'_{111} are similar to those for the S_0^L leptoquark, but here the gauge decay contributes dominantly at low coupling (i.e. $M_{\tilde{q}} \leq 100$ GeV) and the $\not{R}_p$ decay at masses ≥ 175 GeV. Masses close to the kinematic limit are reached for $\lambda'_{111} \approx 1$, and couplings 4 times lower than the electromagnetic

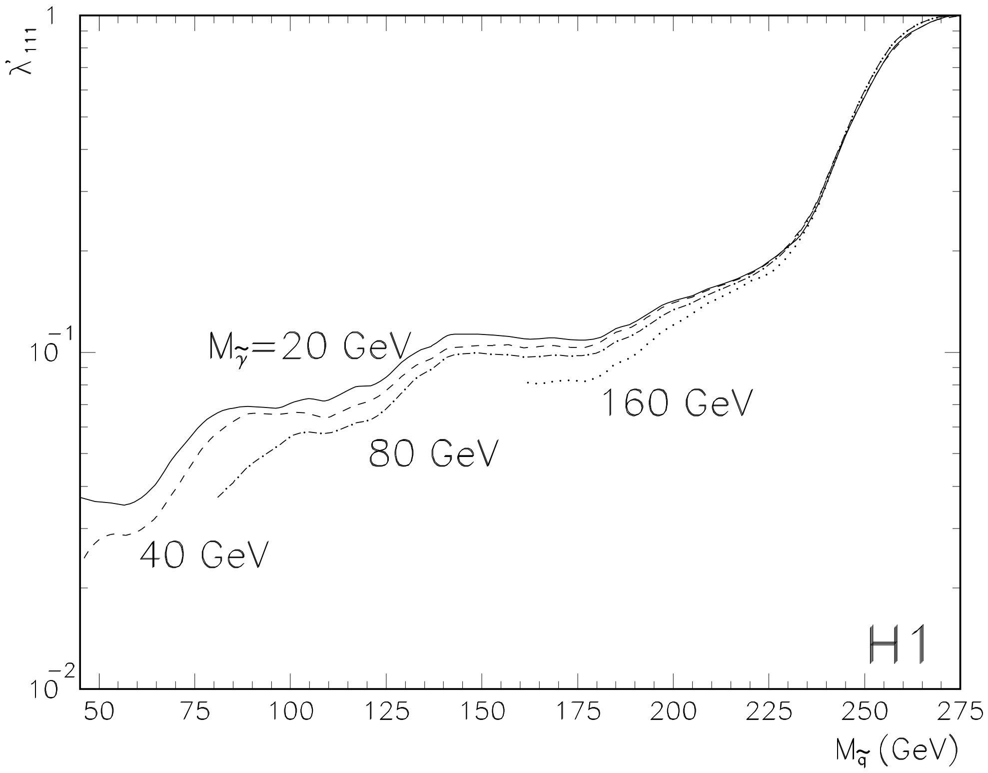

Figure 10: *Upper limits at 95% CL for the coupling λ'_{111} as a function of squark mass for various fixed photino masses. The limits combine all charged and neutral decays of the $\tilde{d}$ and $\bar{\tilde{u}}$.*

coupling are probed for masses around 100 GeV. The limit presented here can also be used in case other squark decays are possible by multiplying the value on λ'_{111} with the square root of the sum of the branching ratios of the decay channels analysed here.

In comparison, the dilepton data from the Tevatron experiments have been used to estimate [32] a mass limit for squarks in the $\not{R}_p$ model of $M_{\tilde{q}} > 100$ GeV. At HERA, a discovery of such particles is thus still possible. Indirect limits obtained from CC universality are close to the results obtained here [33].

In the MSSM there exists the interesting possibility of a large mass splitting between a light and a heavy stop quark. In $\not{R}_p$ supersymmetric models, the light mass eigenstate of the stop, $\tilde{t}_1$, can be produced in the reaction $e^- + \bar{d} \rightarrow \bar{\tilde{t}}$ via a $\not{R}_p$ Yukawa coupling λ'_{131}. Since the top quark is very heavy the decay $\tilde{t} \rightarrow \chi_1^0 t$ is suppressed. For the decay into the initial lepton and quark, the results obtained for the $\tilde{S}_{1/2}$ leptoquark are directly applicable if other supersymmetric decay channels do not contribute [34]. If this is not the case the limit on λ'_{131} has to be multiplied with the square root of the sum of the branching ratios of the decay channels analysed here. This however only holds if the total intrinsic width of the stop does not exceed the experimental mass resolution of a few GeV.

9 Conclusions

We have searched for leptoquarks, leptogluons and squarks in electron–parton scattering at HERA. Various kinematic reconstruction methods have been investigated to minimize the dependence on higher order QED and QCD radiation in the initial and final state. For the decay modes studied, an electron or neutrino together with jets, the different angular distributions of these processes were used together with the reconstructed particle masses to separate possible signals from the Standard Model deep inelastic scattering process. No striking evidence for the production of new particles was found. Instead mass dependent limits at 95% confidence level for couplings were derived.

Leptoquarks, classified model independent into scalar and vector multiplets, are excluded for couplings of electromagnetic strength ($\lambda = 0.3$) for the following masses (cf. fig. 6):

Table 2:

Type	S_0^L	S_0^R	$\tilde{S}_0^R$	S_1^L	$S_{1/2}^L$	$S_{1/2}^R$	$\tilde{S}_{1/2}^L$
Charge states	-1/3	-1/3	-4/3	-4/3, -1/3	-5/3	-5/3, -2/3	-2/3
Mass limits (GeV)	230	223	204	235	133	148	139
Type	$V_{1/2}^L$	$V_{1/2}^R$	$\tilde{V}_{1/2}^L$	V_0^L	V_0^R	$\tilde{V}_0^R$	V_1^L
Charge states	-4/3	-4/3, -1/3	-1/3	-2/3	-2/3	-5/3	-5/3,-2/3
Mass limits (GeV)	206	230	226	142	148	144	180

Beside this resonance search, a contact interaction analysis for interference between leptoquark exchange and Standard Model gauge boson exchange revealed good agreement of data and the Standard Model expectation. From these results additional limits in terms of mass/coupling are established for $\tilde{V}_0^R$, $V_{1/2}^R$, $\tilde{V}_{1/2}^L; V_1^L$ to be below $397, 297, 320, 531$ GeV respectively.

Leptogluon masses below 169 GeV are excluded for compositeness scales up to 1 TeV (cf. fig. 7).

Squarks, in the $\not{R}_p$ violating extension of supersymmetry, couple to lepton–quark pairs, but may equally well decay into a quark and a photino, with subsequent 3-body decays of the photino. Making explicit use of this lepton number violating mode, no evidence for squark production was found and photino mass dependent limits of $M_{\tilde{q}} \gtrsim 239$ GeV are obtained for couplings of electromagnetic strength (cf. fig. 10).

For all these particles the results obtained here enter a previously unexplored region in the mass–coupling space for direct particle searches.

Acknowledgements

We are grateful to the HERA machine group whose outstanding efforts made this experiment possible. We appreciate the immense contributions of the engineers and technicians who constructed and maintained the detector. We thank the funding agencies for financial support. We acknowledge the support of the DESY technical staff. We also wish to thank the DESY directorate for the hospitality extended to the non-DESY members of the H1 Collaboration.

References

[1] H1 Collaboration, I. Abt et al., Nucl. Phys. B396 (1993) 3.

[2] ZEUS collaboration, M. Derrick et al., Phys. Lett. B306 (1993) 173.

[3] W. Buchmüller, R. Rückl and D. Wyler, Phys. Lett. B191 (1987) 442.

[4] B. Schrempp, Proc. of the Workshop Physics at HERA, DESY, Hamburg (1991), vol. 2 p. 1034, and references therein.

[5] S. Davidson, D. Bailey and B. Campbell, Z. Phys. C61 (1994) 613;
M. Leurer, Phys. Rev. D49 (1994) 333; *ibid.* D50 (1994) 536.

[6] H. Fritzsch and G. Mandelbaum, Phys. Lett. B102 (1981) 319;
U. Baur and K.H. Streng, Z. Phys. C30 (1986) 325.

[7] J. Bijnens, Proc. of the HERA Workshop, DESY, Hamburg (1987), vol. 2 p. 819. The lagrangian here is multiplied by 1/2 in order to comply with the more common definition.

[8] L.E. Ibáñez and G.G. Ross, Nucl. Phys. B368 (1992) 3.

[9] For reviews see H.P. Nilles, Phys. Rep. 110 (1984) 1;
H.E. Haber and G.L. Kane, Phys. Rep. 117 (1985) 75.

[10] J. Butterworth and H. Dreiner, Nucl. Phys. B397 (1993) 3, and references therein.

[11] P. Haberl, F. Schrempp and H.-U. Martyn, Proc. of the Workshop Physics at HERA, DESY, Hamburg (1991), vol. 2 p. 1133.

[12] E. Eichten, K. Lane and M.E. Peskin, Phys. Rev. Lett. 50 (1983) 811.

[13] R. Rückl, Phys. Lett. B129 (1983) 363; *idem* Nucl. Phys. B234 (1984) 91.

[14] H1 Collaboration, I. Abt et al., DESY preprint 93-103 (July 1993).

[15] H1 Calorimeter Group, B. Andrieu et al., Nucl. Instr. and. Meth. A336 (1993) 460.

[16] H1 Calorimeter Group, B. Andrieu et al., DESY preprint 94-055 (March 1994);
idem, Nucl. Instr. and. Meth. A336 (1993) 499.

[17] LEGO 0.02 and SUSSEX 1.5; K. Rosenbauer, thesis RWTH Aachen, PITHA report to be published.

[18] PYTHIA 5.6; T. Sjöstrand, Comp. Phys. Comm. 39 (1986) 347;
T. Sjöstrand and M. Bengtsson, Comp. Phys. Comm. 43 (1987) 367;
JETSET 7.3; T. Sjöstrand, CERN preprint TH-6488-92 (1992).

[19] LEPTO 6.1; G. Ingelman, Proc. of the Workshop Physics at HERA, DESY, Hamburg (1991), vol. 3 p. 1366.

[20] DJANGO 2.1; G.A. Schuler and H. Spiessberger, Proc. of the Workshop Physics at HERA, DESY, Hamburg (1991), vol. 3 p. 1419.

[21] A.D. Martin, W.J Stirling and R.G. Roberts, Phys. Rev. D47 (1993) 867.

[22] H1 Collaboration, I. Abt et al., Nucl. Phys. B407 (1993) 515,
ZEUS Collaboration, M. Derrick et al., Phys. Lett. B316 (1993) 412.

[23] M. Glück, E. Reya and A. Vogt, Phys. Rev. D45 (1992) 3986; *ibid.*, D46 (1992) 1973.

[24] H1 Calorimeter Group, B. Andrieu et al., Nucl. Instr. and Meth. A344 (1994) 492.

[25] H1 Collaboration, T. Ahmed et al., Phys. Lett. B324 (1994) 241.

[26] Particle Data Group, Phys. Rev. D45 (1992) part II.

[27] M. Glück, E. Reya and A. Vogt, Z. Phys. C53 (1992) 127; *idem*, Phys. Lett. B306 (1993) 391.

[28] J.G. Morfín and W.-K. Tung, Z. Phys. C52 (1991) 13.

[29] W. Merritt, D0 Collaboration, Proc. of the XXIXth Rencontre de Moriond (1994), to be published;
D0 collaboration, S. Abachi, Phys. Rev. Lett. 72 (1994) 965;
CDF collaboration, F. Abe, Phys. Rev. D48 (1993) 3939.

[30] U. Baur and K.H. Streng, Phys. Lett. B162 (1985) 387.

[31] A.D. Martin, W.J. Stirling and R.G. Roberts, Phys. Lett. B306 (1993) 145; *ibid.*, B309 (1993) 492.

[32] D.P. Roy, Phys. Lett. B283 (1992) 270.

[33] V. Barger, G.F. Giudice and T. Han, Phys. Rev. D40 (1989) 2987.

[34] T. Kon, T Kobayashi and S .Kitamura, Phys. Lett. B333 (1994) 263.